

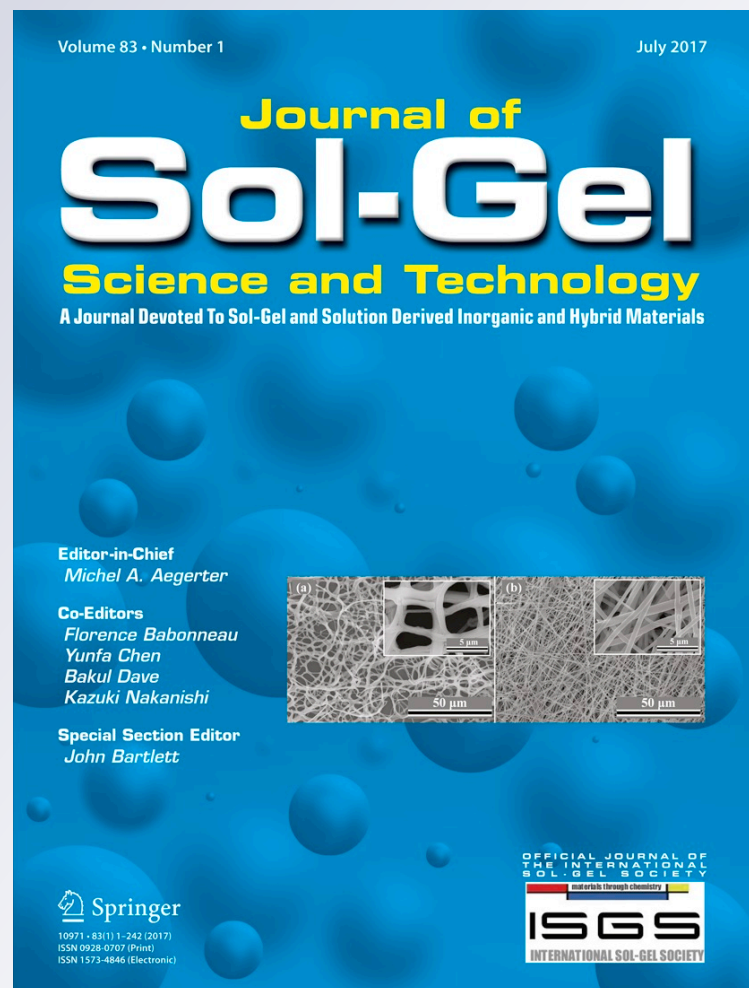
Permeation and optical properties of YAG:Er³⁺ fiber membrane scintillators prepared by novel sol-gel/electrospinning method

**Zhaoxi Chen, Artem A. Trofimov, Luiz
G. Jacobsohn, Hai Xiao, Konstantin
G. Kornev, Dong Xu & Fei Peng**

**Journal of Sol-Gel Science and
Technology**

ISSN 0928-0707
Volume 83
Number 1

J Sol-Gel Sci Technol (2017) 83:35-43
DOI 10.1007/s10971-017-4387-y



Your article is protected by copyright and all rights are held exclusively by Springer Science +Business Media New York. This e-offprint is for personal use only and shall not be self-archived in electronic repositories. If you wish to self-archive your article, please use the accepted manuscript version for posting on your own website. You may further deposit the accepted manuscript version in any repository, provided it is only made publicly available 12 months after official publication or later and provided acknowledgement is given to the original source of publication and a link is inserted to the published article on Springer's website. The link must be accompanied by the following text: "The final publication is available at link.springer.com".

Permeation and optical properties of YAG:Er³⁺ fiber membrane scintillators prepared by novel sol–gel/electrospinning method

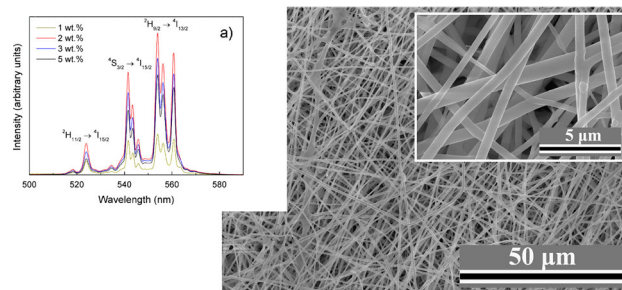
Zhaoxi Chen¹ · Artem A. Trofimov¹ · Luiz G. Jacobsohn^{1,2} · Hai Xiao³ · Konstantin G. Kornev¹ · Dong Xu⁴ · Fei Peng^{1,2} 

Received: 5 February 2017 / Accepted: 5 April 2017 / Published online: 22 April 2017
© Springer Science+Business Media New York 2017

Abstract An electrospinning method for fabrication of the YAG:Er³⁺ fibrous membrane is developed and the scintillation properties of the obtained membranes were examined. A homogeneous precursor YAG sol was synthesized allowing to control the sol–gel transition. The synthesized precursor allows one to achieve the 5 wt.% level of fiber doping with Er without formation of any undesired crystalline phases. It was found that the relative humidity had a strong impact on the fiber microstructure. The fibers obtained at the low relative humidity level (~30%) had almost straight cylindrical shape with an average diameter of ~590 nm, their surface was smooth. The shape of fibers obtained at the high relative humidity level (~50%) deviated from the straight cylindrical shape and the average diameter was larger, ~1.12 μm. The fluid permeability of membranes, K, obtained at the low relative humidity level was measured using an upward wicking experiment to give $K \sim 10^{-13} \text{ m}^2$. The YAG:Er membrane presented a strong green photoluminescence under ultraviolet excitation and intense

radioluminescence dominated by emission lines at 398 and 467 nm under the X-ray excitation. The properties of these materials make them promising candidates as porous scintillators for the detection of ionizing radiation of flowing fluids.

Graphical Abstract



Keywords YAG:Er fiber · Fluid transport · Luminescence · Porous scintillator

Zhaoxi Chen and Artem A. Trofimov contributed equally to this work.

✉ Luiz G. Jacobsohn
luiz@clemson.edu

✉ Fei Peng
fpeng@clemson.edu

¹ Department of Materials Science and Engineering, Clemson University, Clemson, SC 29634, USA

² COMSET, Center for Optical Materials Science and Engineering Technologies, Clemson University, Anderson, SC 29635, USA

³ Department of Electrical and Computer Engineering, Clemson University, Clemson, SC 29634, USA

⁴ School of Material Science and Engineering, Jiangsu University, No. 301 Xuefu Road Zhenjiang 212013, China

1 Introduction

Bulk single-crystalline and polycrystalline ceramic scintillators have been widely used as sensors for the detection and measurement of ionizing radiation in many fields, from medical imaging to security and high energy physics, but they have limited applicability for the detection of alpha-emitting and beta-emitting radioactive sources dispersed in fluids due to the short range of these radiations in matter. In fact, most of the volume of bulk scintillators does not contribute for the detection of alpha and beta radiation. On the other hand, while the use of porous ceramic scintillators has advantages for this application, it has received

limited attention [1]. Current methods for the detection of radioactive species in water, for example, require in situ extraction and shipping of samples, as well as ex situ analysis, a process that consumes several days. On the other hand, the proposed porous scintillator can be used for instantaneous and continuing in situ monitoring. Additionally, the demand for photoluminescent ceramic fibers has increased significantly motivated by the development of nanolasers, nanowaveguides, and other miniaturized electronic and photonic devices, particularly ultra-high performance sensors [2–4], as well as by the large active area of the ceramic membranes. Within this context, yttrium aluminum garnet (YAG)-based fiber membrane scintillators are proposed and evaluated due to their unique advantages of fluid permeability and mechanical robustness [5–7]. The choice of YAG relies on this material exhibiting exceptional optical transparency, having a cubic crystallographic structure that can accommodate dopants, and being a well-known scintillator used in electron microscopy, phosphor for lighting, and solid state laser medium when properly activated with rare earth ions [8, 9].

Electrospinning is a versatile technique capable of making continuous ceramic fibers that has been extended to make porous ceramic membranes with small pore size and narrow pore size distributions [10–12]. In the sol–gel process, ceramics materials can be prepared from alkoxide precursors, which hydrolyze in acidic water-based solutions to form linear polymeric structures [13–15]. This sol–gel method is capable of making continuous thick fibers typically with diameters in the micrometer range [14, 16, 17]. A combination of the sol–gel and electrospinning methods has been employed to produce ceramic fibers [18–20]. In general, polymer spin-aids are added to the pre-spinning solution to improve fiber formation and the use of polyvinyl alcohol, polyvinylpyrrolidone, and polyethylene oxide (PEO) has shown improvement in YAG fiber formation [4, 21–23].

In this work, the fabrication and evaluation of fiber membrane scintillators is carried out as a first step toward their application as high-performance ionizing radiation

fluid sensors. Particular attention is given to the transport properties of liquids, as determined by up-wicking experiments, and the determination of the intrinsic permeability of the YAG membranes.

2 Experimental procedures

2.1 Materials preparation

2.1.1 Preparation of the YAG sol and electrospinning solution

Aluminum isopropoxide (AIP; $\text{Al}(\text{C}_3\text{H}_7\text{O})_3$, 98%, Sigma, MO), aluminum nitrate nonahydrate (AN; $\text{Al}(\text{NO}_3)_3 \cdot 9\text{H}_2\text{O}$, 98%, Alfa Aesar, MA), and yttrium nitrate hexahydrate (YN; $\text{Y}(\text{NO}_3)_3 \cdot 6\text{H}_2\text{O}$, 99.9%, Alfa Aesar, MA) were used to synthesize the YAG precursor. Erbium nitrate pentahydrate (EN; $\text{Er}(\text{NO}_3)_3 \cdot 5\text{H}_2\text{O}$, 99.9%, Sigma, MO) was used as the starting material of the dopant, and deionized (DI) water was used as the solvent. The precursor compositions are given in Table 1. For each batch, the total amount of AIP and AN were kept at 0.05 mole. AN and YN were dissolved in DI water at room temperature by vigorously stirring for 30 min. The molar ratio between YN and DI water was kept at 3:100. AIP was then added into the solution and stirred for 24 h, followed by refluxing at 80 °C for 5 h. Specific amounts of EN were then added to the YAG sol after the refluxing at 80 °C such that the concentration of Er_2O_3 was 1, 2, 3, and 5 wt. % of YAG, respectively. Approximately, 2/3 of the solvent was removed using a rotary evaporator (IKA RV 10 digital, IKA, China). These solutions were heated in an oven set at 80 °C until viscous sols were formed. The concentration process took approximately 24 h. The viscosity of the sol was further adjusted by the addition of an ethanol:water mixture with ~42:3 weight ratio to facilitate the electrospinning process. The diluted solution had a ceramic yield of ~6.5 wt. %. PEO (MW 1,000,000, Aldrich, MO) was then added up to 0.5–2 wt. % to the diluted YAG:Er sol to improve fiber formation.

Table 1 Fabrication conditions and sol formation of samples investigated in this work

Sample #	AIP:AN:YN	pH after reflux	Sol appearance	
			After reflux	After condensation
1	5:0:3	3.0	White and opaque	Precipitate
2	4.5:0.5:3	2.5	White and opaque	Precipitate
3	4:1:3	2.1	Gray and opaque	Precipitate
4	3.75:1.25:3	2.1	Gray and transparent	Jelly
5	3.5:1.5:3	1.8	Transparent	Transparent solid
6	3.25:1.75:3	1.8	Transparent	Translucent solid
7	3:2:3	1.8	Transparent	Translucent solid

2.1.2 Electrospinning and heat treatment

The fibers were electrospun under an applied electrical field generated using a high voltage supply (Model PS/FC60P02.0-11, Glassman High Voltage Inc, NJ). A positive voltage of 10 kV was applied to the needle of the syringe containing solutions for electrospinning driven by a syringe pump (Model NE-300, New Era Pump System Inc, NY). The flow rate was set to about 0.5 mL/h, and the needle was placed 20 cm apart from the collector. The ambient relative humidity (RH) was recorded during electrospinning. For examination of the fiber morphology, a thin fiber membrane was collected on a silicon substrate after electrospinning for 30 s. Thick fiber membranes were collected after electrospinning for 2 h. The fibers were cut from the collector, collected in the form of free-standing membranes, and dried in a desiccator for 24 h. Heat treatment was carried out with heating rate of 1 °C/min up to 500 °C and 5 °C/min up to the target temperature, either 1000 or 1200 °C, where fibers were kept for 2 h.

2.2 Characterization

The thermal characteristics of the membranes were studied at different heating rates under air flow through differential thermal analysis (DTA) using a DTA7 analyzer (Perkin Elmer, MA), and through thermogravimetric analysis (TGA) using a TGA7 analyzer (Perkin Elmer, MA). The crystalline phases were identified by X-ray diffraction (XRD) using a Ultima IV diffractometer (Rigaku, Japan). Fiber morphology was characterized by scanning electron microscopy (SEM) using a S4800 microscope (Hitachi, Japan).

Permeability was evaluated by means of the upward-wicking experiments [24]. The experimental setup used is schematically shown in Fig. 1. The membranes were clipped into small rectangular pieces 2–3 mm wide and 10 mm

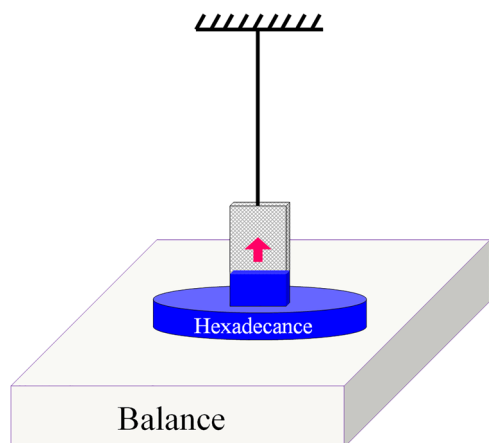


Fig. 1 Schematics of the setup for the up-wicking experiments

long, with the cross-sectional area of the membrane being measured with a microscope. The membrane was suspended above a container partially filled with hexadecane (density: 0.773 g/cm³; viscosity: 3.3 cp; surface tension: 27 mN/m) placed on top of a microbalance (LE26P, Sartorius, Germany). Once the bottom of the membrane was placed in contact with hexadecane, the weight change was monitored and continuously recorded as a function of time. The porosity (ϕ) of the membrane was calculated from the weight of the membrane before and after the wicking experiment using the following formula:

$$\phi^{-1} = \frac{\text{Weight before}}{\text{Weight after} - \text{Weight before}} \times \frac{\rho_{\text{hex}}}{\rho_{\text{YAG}}} + 1, \quad (1)$$

where ρ_{hex} and ρ_{YAG} are the density of hexadecane and YAG (4.56 g/cm³), respectively.

Photoluminescence (PL) spectra were obtained using a Horiba Jobin Yvon Fluorolog 3 spectrofluorometer equipped with double monochrometers for both excitation and detection, and a 450 W xenon lamp as the excitation source. All measurements were carried out in ambient conditions with excitation set at 381 nm and detection spectral resolution of 1 nm. Spectra were not corrected for the spectral sensitivity of the system.

Scintillation was evaluated by means of radioluminescence (RL) measurements under X-ray excitation using a custom-designed Lexsyg Research spectrophotometer (Freiberg Instruments, Germany) equipped with a VF-50J X-ray tube (Varian Medical Systems, UT) with a W target and operated at 40 kV and 1 mA, and a DU920P-BU Newton CCD camera (Andor Technology, UK). Spectra were not corrected for the spectral sensitivity of the system.

3 Results and discussion

3.1 Sol formation

The composition of the precursor and the conditions for YAG sol formation, including the pH values after condensation, are summarized in Table 1. The sol–gel method is sensitive even to small changes in the processing parameters such as the pH value, the content of organic and inorganic salts, and the content of water, any of them capable of leading to significant differences in the sol character [25]. Moreover, the homogeneity of the mixed species is usually evaluated by the transparency of the resultant sol [25]. For samples #1 to 3, the metal alkoxide precursors were not completely miscible and precipitation ahead of gelation was observed, while for sample #4 a jelly-like gel was obtained after condensation suggesting the formation of colloidal species [26]. Samples #6 and 7 were translucent with the presence of flocculates suggesting degraded

homogeneity. Sample #5 remained transparent throughout the sol–gel transition process, and therefore was selected for further investigation.

3.2 Thermal decomposition and phase formation

Figure 2 shows the DTA and TGA results of YAG sol sample #5. The endothermic peaks in DTA curve at temperatures between 100 and 300 °C are due to the evaporation of absorbed solvent and decomposition of low molecular weight molecules. The second main decomposition at temperatures between 300 and 450 °C is attributed to the elimination of alkoxy and nitrate groups [27]. The strong exothermic peak observed at around 920 °C corresponds to the crystallization of YAG [9]. The TGA curve confirms that major weight loss occurred at temperatures below 450 °C, with a total weight loss of approximately 65%.

3.3 Fiber morphology and structure identification

Figure 3 shows optical microscopy images of fibers collected on silicon substrate for the evaluation of the spinnability of the precursor solutions before heat treatment. In the case of solution with 0.5 wt.% PEO, discontinuous jets or droplets were collected due to Rayleigh instability [28]. The increase of PEO concentration in the solution improved fiber formation. This is illustrated for the case of the sample obtained from the solution containing 1 wt.% PEO, where a less developed shish-kebab morphology was observed [29]. For the solution with 1.5 wt.% PEO, fibers are straight and uniform and, therefore, this concentration was selected for the fabrication of fiber membranes.

SEM micrographs of a fiber membrane heat treated at 1000 °C are shown in Fig. 4. It was found that the formation of the fiber membrane was affected by the RH level during electrospinning. For the sample prepared at high RH level (~50%), the fiber membrane consists of a highly

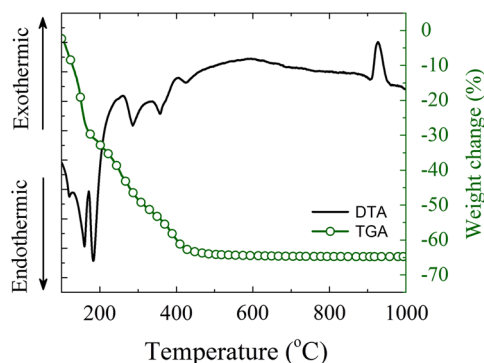


Fig. 2 DTA and TGA results of YAG sample #5. See text for sample details

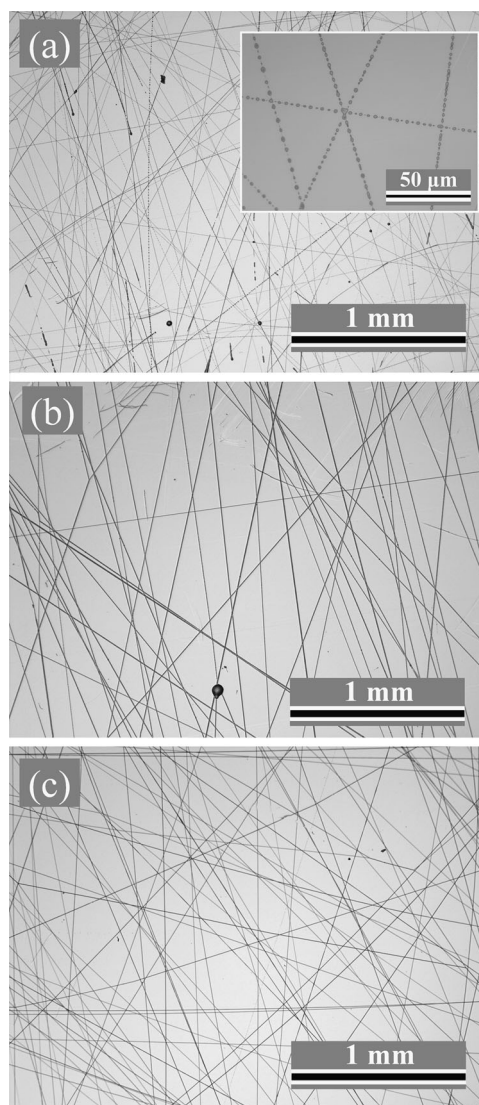


Fig. 3 Optical microscopy images of YAG fibers collected on silicon substrates before heat treatment to demonstrate the effect of PEO concentration: **a** 0.5, **b** 1, and **c** 1.5 wt.%

interconnected fibrous network constituted of bowed fibers with the fibers fused at the contact points. On the other hand, in the case of low RH level (~30%) e-spinning, the fibers in the network appeared straight and, most likely, did not fuse at the points of contacts. The differences in the two fiber networks were attributed to the hygroscopic nature of precursor salts used in this work that absorbed moisture from the environment. Figure 5 shows the statistical distribution of the electro-spun fiber diameter obtained at low and high RH levels. For the low RH level, a narrow distribution was found, with an average diameter of 590 nm and a standard deviation of 190 nm. For the high RH level, a considerably broader distribution of fiber diameter was obtained. The average diameter was about 1.12 μm with a standard deviation of 0.53 μm. Thus, the high RH level

Fig. 4 SEM micrographs of YAG fiber membranes obtained from an electro-spinning solution containing 1.5 wt. % PEO. The fiber membranes were electro-spun at different relative RH levels, **a** ~50%, and **b** ~30%, and heat treated at 1000 °C

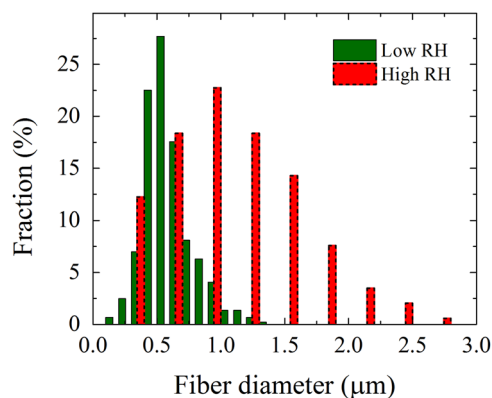
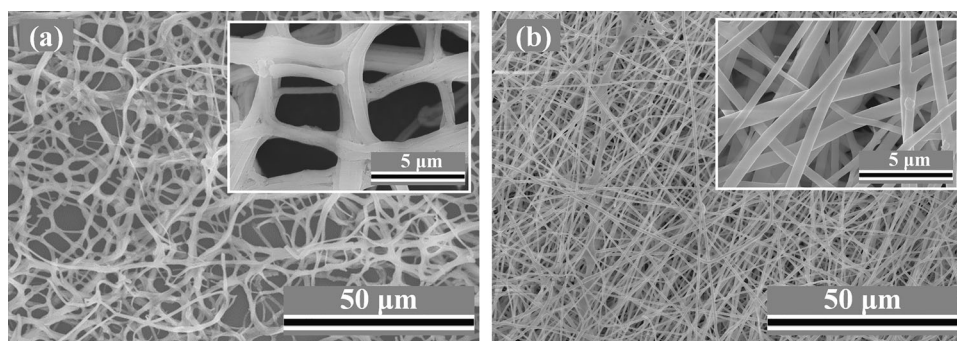


Fig. 5 Statistical distribution of the fiber diameter obtained at high RH (50%) and low RH (30%)

fibers are about two times greater than those obtained at low RH. The larger fibers obtained at the high RH level might have been formed by fusion of 2–3 fibers together during the electrospinning process.

Once the best electro-spinning conditions were found, the effect of heat treatment of the fiber membranes was investigated. In Fig. 6a, the XRD patterns of undoped YAG fibers prepared with 1.5 wt.% PEO, at RH level of 30 %, and heat-treated at different temperatures are shown. No sign of crystallinity was observed after the temperature increase up to 900 °C, while crystallization occurred between 900 and 1000 °C (see Fig. 2, DTA curve). No intermediate phases, such as YAlO_3 (YAP) and $\text{Y}_4\text{Al}_2\text{O}_9$ (YAM) were observed after crystallization [30]. After heat treatment at 1000 and 1200 °C, the XRD results showed the well-defined diffraction peaks and the lack of spurious intermediate phases. Figure 6b shows that Er doping up to 5 wt.% did not lead to the creation of secondary phases, and that YAG remained the only crystalline phase (PDF card no. 33–40). The achievement of the pure YAG phase is important for the optimization of the luminescence and scintillation properties of membranes. The SEM images of surface of the YAG fibers heat treated at 1000 and 1200 °C are shown in Fig. 7. The fibers heat-treated at 1000 °C had a fine microstructure with grain sizes of ~30 nm, while the

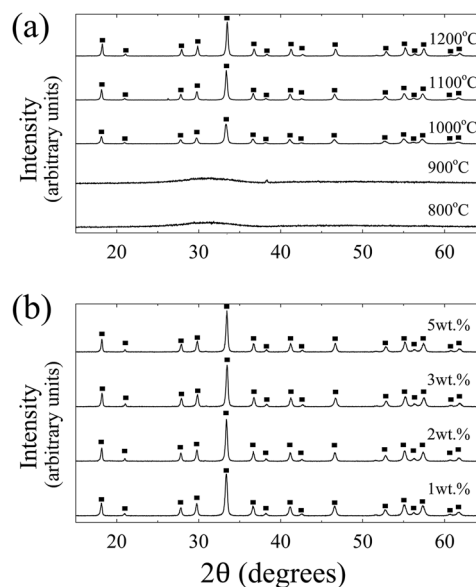


Fig. 6 XRD patterns of YAG gel derived from sol #5 **a** after heat treatment at different temperatures, and **b** doped with different amounts of Er_2O_3 followed by heat treatment at 1200 °C. Labeled phase: YAG (JCPDS#: 33–40)

fibers heat treated at 1200 °C had the grain sizes of ~100 nm and a correspondingly much rougher surface.

In the sol–gel processing, one of the most important issues is the achievement of the desired phase at low temperatures without the formation of intermediate or secondary phases. In our previous studies, we demonstrated that monophasic sol can be developed with the careful control of the hydrolysis and polycondensation reactions [29]. Without careful control of the sol–gel process, an undesired phase can be formed prior the desired phase, requiring higher temperature heat treatment after synthesis. Our previous work on the sol–gel fabrication of mullite fibers showed that if the Al–Si spinel phase is formed prior to the mullite phase, the mullite phase can only be obtained with heat treatments above about 1400 °C. On the other hand, pure mullite phase can be obtained at about 1000 °C using a monophasic gel. In this work, the hydrolysis and

Fig. 7 SEM images of fibers heat treated at **a** 1000 °C, and **b** 1200 °C

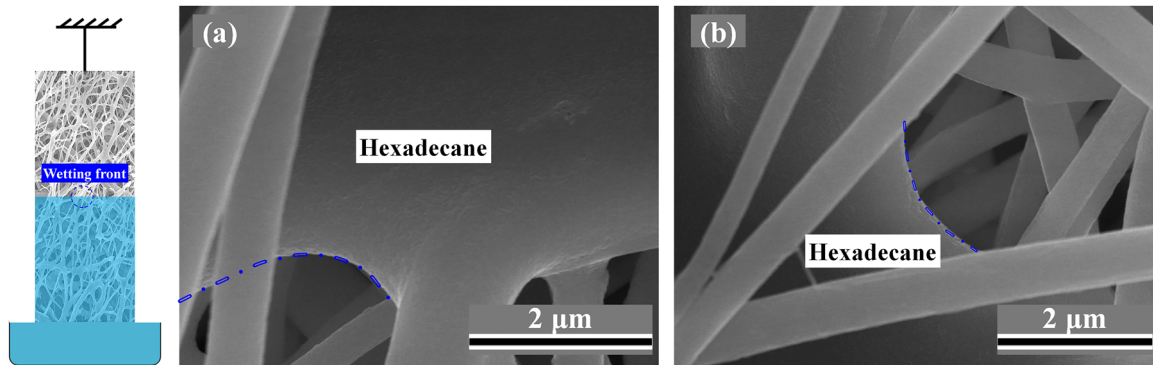
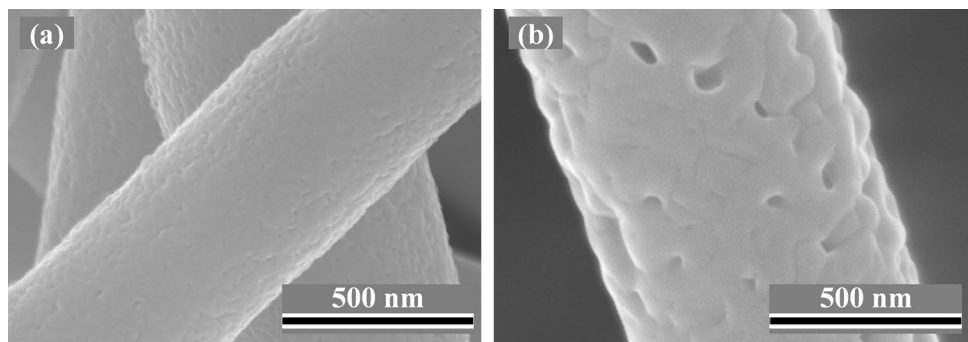


Fig. 8 SEM images showing the meniscus of the wicking liquid in the fiber membrane. The curvature was estimated by generating normal lines to the meniscus. The *left* image shows schematically the wicking front

polycondensation process is similar to the case of mullite. A mild acidic chemical environment is beneficial to the formation of a homogeneous sol. Basic or not enough acidic conditions usually lead to diphasic sol or precipitation [29], while excessive acidic conditions tend to result in uncontrollable gelation [25]. Through careful manipulation of the synthesis conditions, it was possible to obtain phase pure and fine-grained YAG at 1000 °C, without the need of heat treatments at higher temperatures.

3.4 Permeability of YAG fiber membrane

The underpinning goal of this work is the development of fiber membrane scintillators for the detection of ionizing radiation from flowing fluids. In order to evaluate the permeability of these materials, we heat treated the membranes, which were processed under the same conditions at 1200 °C and carried out the upward-wicking experiments [24, 31, 32]. The Lucas–Wasburn equation describing the rate of advance of the wetting front is given by [31, 32]:

$$\frac{dL}{dt} = \frac{k}{\eta\phi} \times \frac{1}{L} (P_c - \rho gL), \quad (2)$$

where L is the position of the wicking front at time t , k is the permeability, ϕ is the porosity of the membrane, P_c is the capillary pressure, η and ρ are the viscosity and density of

the liquid, respectively, and g the gravitational constant. The capillary pressure was estimated from the radius R of meniscus and surface tension σ of the liquid using the Young–Laplace equation: $P_c = \frac{2\sigma}{R}$. Figure 8 shows a typical meniscus shape and R was estimated to be in the micrometer range ($\sim 2 \mu\text{m}$), which is close to the average pore size. Porosity was measured to be 80–90%, slightly greater than the porosity of polymer fiber webs ($\sim 60\text{--}70\%$) reported elsewhere [33]. It is noted that the experimental error in porosity (up to 10%) does not change the magnitude of the calculated permeability value.

For fibrous materials, the driving force (capillary pressure) is expected to be much greater than the hydrostatic pressure, and thus the gravitational effects can be ignored [33]. In these conditions, the solution to the Lucas–Wasburn Eq. (1) is simplified to [33]:

$$L^2 = \frac{2P_c k}{\eta\phi} t + C, \quad (3)$$

where C is an integration constant determined by the initial conditions. The weight of liquid within the fiber membrane is $m = \rho AL\phi$, where A is the area of the through-membrane-thickness cross-section. The mass of liquid absorbed by the membrane over time period t is calculated from Eq. (2) as:

$$m^2 = \frac{2P_c \rho^2 A^2 \phi k}{\eta} t + C \rho^2 A^2 \phi^2, \quad (4)$$

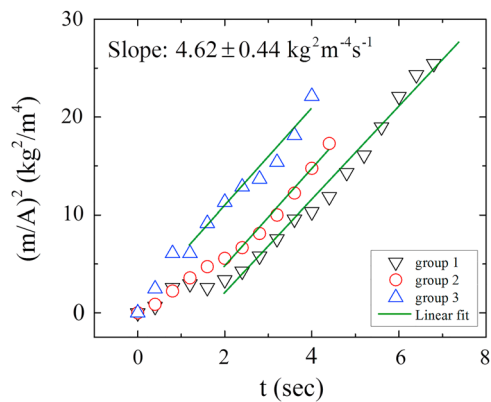


Fig. 9 Variation of the m^2/A^2 ratio as a function of time for three different fiber membranes processed under the same conditions (to check for the reproducibility of the upward-wicking experiment). The simplified Lucas–Washburn model was applied to fit the data

Figure 9 shows the plot of m^2/A^2 as a function of time for the YAG fiber membrane obtained at the low RH levels. From the slope of the best linear fit to the data points, the permeability k was calculated. The estimate of the permeability based on three independent measurements is $(5.6 \pm 0.5) \times 10^{-13} \text{ m}^2$, which falls within the range of permeabilities found in the electrospun fibrous mats and nanofiber yarns [33]. In the case of the YAG membrane obtained at the high RH levels, difficulties in obtaining good free-standing samples hindered the execution of the upward-wicking tests.

3.5 Luminescence

PL results are presented in Fig. 10 for YAG precursor powders activated with 1, 2, 3 and 5 wt.% Er and heat treated at 1200 °C. A series of strong emission lines from 510 to 580 nm originated in the $^2\text{H}_{11/2} \rightarrow ^4\text{I}_{15/2}$, $^4\text{S}_{3/2} \rightarrow ^4\text{I}_{15/2}$, and $^2\text{H}_{9/2} \rightarrow ^4\text{I}_{13/2}$ transitions [34, 35] were observed (Fig. 10a), in addition to a series of weak emission lines between 630 and 690 nm assigned to the $^4\text{F}_{9/2} \rightarrow ^4\text{I}_{15/2}$ transition [34] (not shown in Fig. 10a). The increase of Er content is known to affect the relative intensity of the emission lines of YAG:Er, promoting green and red at the expense of the UV-blue emission for increasing Er concentrations from 0.735 to 6.6 at.% [36]. The decrease of Er concentration from 20.57 to 0.778 at.% showed an increase in the spontaneous radiative transition rate of the transitions $^2\text{H}_{11/2} \rightarrow ^4\text{I}_{15/2}$ and $^4\text{S}_{3/2} \rightarrow ^4\text{I}_{15/2}$, while the rate for the $^2\text{H}_{9/2} \rightarrow ^4\text{I}_{13/2}$ transition remained fixed [35]. In Fig. 10b, PL intensity of the green emission as determined by the intensity integration over the 500–600 nm range is shown. Since the integrated intensity curve exhibited a maximum at 2 wt.%, scintillation was evaluated under X-ray excitation for this particular composition. A typical RL spectrum is

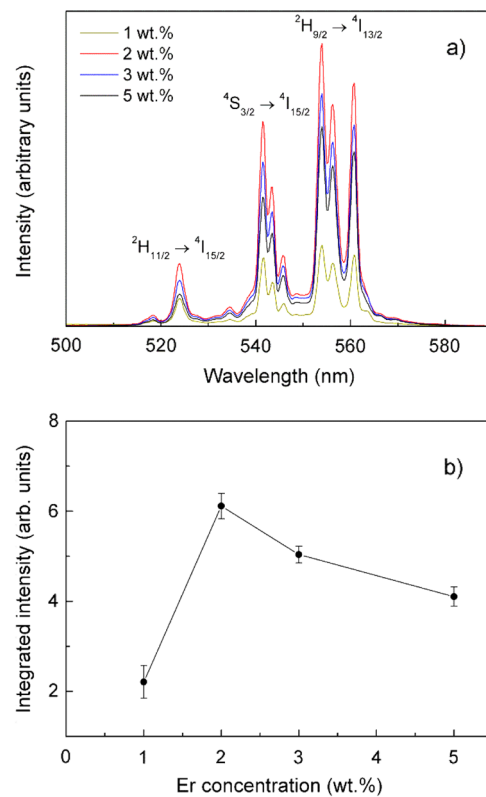


Fig. 10 a PL spectra of YAG:Er powders with different Er concentrations heat treated at 1200 °C. b Integrated PL intensity as a function of Er concentration

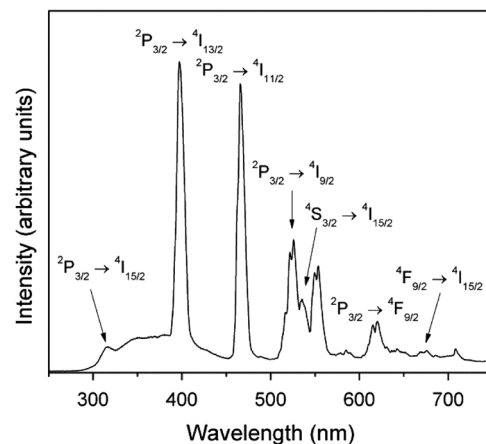


Fig. 11 Radioluminescence spectrum of YAG:Er powders doped with 2 wt.% Er heat treated at 1200 °C. The electronic transitions of the main emission lines are shown

shown in Fig. 11, where a number of lines are observed. The lines were assigned to specific electronic transitions based on the results of cathodoluminescence measurements of YAG:Er single crystalline films grown by the liquid phase epitaxy method [36], as shown in Fig. 11. A broad band from about 300 to 450 nm was also observed and

ascribed to the combined contribution of the ${}^2P_{3/2} \rightarrow {}^4I_{15/2}$ transition with the emission of F, F⁺, and Y_{Al} antisite defects [37, 38]. More importantly, RL was dominated by emission lines at 398 and 467 nm that match the maximum detection efficiency of photomultiplier tubes. In summary, these results demonstrated the luminescence functionality of this material.

4 Conclusions

The fabrication and evaluation of Er-doped YAG fiber membrane scintillators was carried out. Samples were prepared by the combined sol–gel/electrospinning method. It was found that addition of 1.5 wt.% PEO to the precursor sol improved the formation of ceramic fibers during electrospinning. It was also found that environmental humidity played a major role in the formation of a strong membrane with a controllable pore size. The best e-spun membranes were obtained at the low RH values of ~30%. A post-fabrication heat treatment at 1000 °C yielded a pure YAG phase fiber membranes. The permeability of these membranes was found to be on the order of $5.6 \times 10^{-13} \text{ m}^2$. It was also demonstrated that the YAG:Er membrane with 2 wt.% Er exhibited a strong luminescence under UV and X-ray excitations. The obtained results show a great potential for the YAG:Er e-spun membranes as porous scintillators for detection of ionizing radiation in fluids either still or flowing.

Acknowledgements This work is supported by the Department of Energy under grant DE-FE00012272 and the National Science Foundation under Grant No. 1207080.

Compliance with ethical standards

Conflict of interest The authors declare that they have no conflict of interest.

References

- Keillor ME, Burggraf LW (1997) Detecting alpha radiation by scintillation in porous materials. *IEEE Trans Nucl Sci* 44 (5):1741–1746
- Lu W, Lieber CM (2007) Nanoelectronics from the bottom up. *Nat Mater* 6(11):841–850
- Huang MH et al. (2001) Room-temperature ultraviolet nanowire nanolasers. *Science* 292(5523):1897–1899
- Dong G et al. (2010) Size-dependent polarized photoluminescence from Y₃Al₅O₁₂: Eu³⁺ single crystalline nanofiber prepared by electrospinning. *J Mater Chem* 20(8):1587–1593
- Park SJ, Chase GG, Jeong KU, Kim HY (2010) Mechanical properties of titania nanofiber mats fabricated by electrospinning of sol–gel precursor. *J Solgel Sci Technol* 54(2):188–194
- Zhu L, Gu L, Zhou Y, Cao S, Cao X (2011) Direct production of a free-standing titanate and titania nanofiber membrane with selective permeability and cleaning performance. *J Mater Chem* 21(33):12503–12510
- Feng C, Khulbe KC, Matsuura T, Tabe S, Ismail AF (2013) Preparation and characterization of electro-spun nanofiber membranes and their possible applications in water treatment. *Sep Purif Technol* 102:118–135
- Ikesue A, Kinoshita T, Kamata K, Yoshida K (1995) Fabrication and optical properties of high-performance polycrystalline Nd: YAG ceramics for solid-state lasers. *J Am Ceram Soc* 78 (4):1033–1040
- Pfeifer S, Bischoff M, Niewa R, Clauß B, Buchmeiser MR (2014) Structure formation in yttrium aluminum garnet (YAG) fibers. *J Eur Ceram Soc* 34(5):1321–1328
- Li D, Xia Y (2004) Electrospinning of nanofibers: reinventing the wheel? *Adv Mater* 16(14):1151–1170
- Ramaseshan R, Sundarrajan S, Jose R, Ramakrishna S (2007) Nanostructured ceramics by electrospinning. *J Appl Phys* 102 (11):111101
- Gibson P, Schreuder-Gibson H, Rivin D (2001) Transport properties of porous membranes based on electrospun nanofibers. *Colloids Surf A Physicochem Engi Asp* 187:469–481
- Shojaie-Bahaabad M, Taheri-Nassaj E, Naghizadeh R (2008) An alumina–YAG nanostructured fiber prepared from an aqueous sol–gel precursor: preparation, rheological behavior and spinnability. *Ceram Int* 34(8):1893–1902
- Li C, Zhang Y, Gong H, Zhang J, Nie L (2009) Preparation, microstructure and properties of yttrium aluminum garnet fibers prepared by sol–gel method. *Mater Chem Phys* 113(1):31–35
- Pullar RC, Taylor MD, Bhattacharya AK (1999) The sintering behaviour, mechanical properties and creep resistance of aligned polycrystalline yttrium aluminium garnet (YAG) fibres, produced from an aqueous sol–gel precursor. *J Eur Ceram Soc* 19 (9):1747–1758
- Shojaie-Bahaabad M, Taheri-Nassaj E, Naghizadeh R (2008) An alumina–YAG nanostructured fiber prepared from an aqueous sol–gel precursor: preparation, rheological behavior and spinnability. *Ceram Int* 34(8):1893–1902
- Liu Y, Zhang ZF, Halloran J, Laine RM (1998) Yttrium aluminum garnet fibers from metalloorganic precursors. *J Am Ceram Soc* 81 (3):629–645
- Pirzada T, Arvidson SA, Saquing CD, Shah SS, Khan SA (2012) Hybrid silica–PVA nanofibers via sol–gel electrospinning. *Langmuir* 28(13):5834–5844
- Hou Z et al. (2008) Preparation and luminescence properties of YVO₄: Ln and Y(V,P)O₄: Ln (Ln= Eu³⁺, Sm³⁺, Dy³⁺) nanofibers and microbelts by sol–gel/electrospinning process. *Chem Mater* 20(21):6686–6696
- Choi SS, Lee SG, Im SS, Kim SH, Joo YL (2003) Silica nanofibers from electrospinning/sol–gel process. *J Mater Sci Lett* 22 (12):891–893
- Khalil KA, Almajid AA, El-Danaf EA, El Rayes MM, Sherif ESM (2012) Direct fabrication of yttrium aluminium garnet nanofibers by electrospinning. *Int J Electrochem Sci* 7:12218–12226
- Suryamas AB, Munir MM, Iskandar F, Okuyama K (2009) Photoluminescent and crystalline properties of Y₃-xAl₅O₁₂: Cex³⁺-phosphor nanofibers prepared by electrospinning. *J Appl Phys* 105 (6):064311
- Ma Z et al. (2012) Porous YAG: Nd³⁺ fibers with excitation and emission in the human “NIR Optical Window” as luminescent drug carriers. *Chem Eur J* 18(9):2609–2616
- Tsai CC, Kornev KG (2013) Characterization of permeability of electrospun yarns. *Langmuir* 29(33):10596–10602
- C J Brinker, G W Scherer (2013), *Sol-gel science: the physics and chemistry of sol-gel processing*. Academic press, Boston, MA
- Lloyd GO, Steed JW (2009) Anion-tuning of supramolecular gel properties. *Nat Chem* 1(6):437–442

27. Veith M et al. (1999) Low temperature synthesis of nanocrystalline Y₃Al₅O₁₂ (YAG) and Ce-doped Y₃Al₅O₁₂ via different sol-gel methods. *J Mater Chem* 9(12):3069–3079
28. Zuo W et al. (2005) Experimental study on relationship between jet instability and formation of beaded fibers during electrospinning. *Poly Eng Sci* 45(5):704–709
29. Chen Z et al. (2015) Electrospun mullite fibers from the sol-gel precursor. *J Sol-Gel Sci Technol* 74(1):208–219
30. Xia G, Zhou S, Zhang J, Xu J (2005) Structural and optical properties of YAG: Ce³⁺ phosphors by sol-gel combustion method. *J Cryst Growth* 279(3):357–362
31. Lucas R (1918) Rate of capillary ascension of liquids. *Kolloid Z* 23(15):15–22
32. Washburn EW (1921) The dynamics of capillary flow. *Phys Rev* 17(3):273
33. Callegari G, Tyomkin I, Kornev KG, Neimark AV, Hsieh YL (2011) Absorption and transport properties of ultra-fine cellulose webs. *J Colloid Interface Sci* 353(1):290–293
34. Gruber JB et al. (1993) Energy levels and correlation crystal-field effects in Er³⁺-doped garnets. *Phys Rev B* 48(21):15561
35. Mierczyk Z et al. (2000) Er³⁺ and Yb³⁺ doped active media for 'eye safe' laser systems. *J Alloys Compd* 300:398–406
36. Zorenko Y et al. (2014) Luminescent properties and energy transfer processes in YAG: Er single crystalline films. *J Lumin* 154:198–203
37. Zorenko Y et al. (2007) Exciton and antisite defect-related luminescence in Lu₃Al₅O₁₂ and Y₃Al₅O₁₂ garnets. *Phys Status Solidi B* 244(6):2180–2189
38. Zorenko Y et al. (2010) Luminescence of F⁺ and F centers in Al₂O₃-Y₂O₃ oxide compounds. *IOP Conf Ser Mater Sci Eng* 15(1):012060